Interdisciplinary Research in Medical Sciences Specialty
ISSN: 3062-4401
2024, Volume 4, Issue 2, Page No: 53-66

Available online at: www.galaxypub.co/page/journals

Galaxy Publication

Galaxy Publication

Wavelet Transform Analysis of Continuous Fetal Heart Rate Monitored with a Portable Medical Device

Marek Král[1], Ondřej Veselý[1], Pavel Šimek[1]*

[1]Department of Clinical Data Science, Faculty of Medicine, Masaryk University, Brno, Czech Republic.

***E-mail** ✉ pavel.simek.ds@gmail.com

Received: 06 April 2024; **Revised:** 18 July 2024; **Accepted:** 19 July 2024

ABSTRACT

beat-to-beat tele-fetal monitoring and clinical data comparison using a wavelet transform approach Tele-fetal monitoring represents a significant advancement toward wearable medical devices for pregnant women, enabling comprehensive prenatal care from home. In this study, we implement a wavelet transform algorithm for fetal cardiac monitoring using a portable fetal Doppler device. After evaluating 85 different mother wavelets, the bio-orthogonal 2.2 wavelet at decomposition level 4 was selected for optimal performance. The proposed method was validated using two datasets, including publicly available and clinical recordings. Analysis of PhysioBank data alongside simultaneous clinical measurements demonstrates that the fetal heart rates obtained with our algorithm closely match the reference values, achieving an accuracy exceeding 95%. These findings suggest that the proposed wavelet-based approach provides a reliable and effective method for tele-fetal monitoring, with strong potential for use in similar wearable prenatal care systems.

Keywords: Fetal heart rate, Tele-fetal monitoring, FHR extraction, Wavelet analysis, Signal processing

How to Cite This Article: Král M, Veselý O, Šimek P. Wavelet transform analysis of continuous fetal heart rate monitored with a portable medical device. Interdiscip Res Med Sci Spec. 2024;4(2):53-66. https://doi.org/10.51847/2fww81Ov84

Introduction

Gestation can result in a live birth, spontaneous miscarriage, induced abortion, or stillbirth [1]. Ensuring proper prenatal care and continuous monitoring throughout pregnancy is essential for improving birth outcomes [2]. Clinically, several medical technologies have been developed to monitor fetal heart rate (FHR) during gestation, including cardiotocography (CTG) [3], fetal magnetocardiography (fMCG) [4], fetal electrocardiography (fECG) [5], and fetal scalp electrocardiography (fsECG) [6].

Fetal scalp electrocardiography involves placing electrodes directly on the fetal scalp, providing high signal-to-noise ratio (SNR) recordings. However, it is invasive, can only be used during labor, increases the risk of infection, and requires a skilled clinician for electrode placement [6].

Among non-invasive options, fMCG is recognized for its high SNR by recording the fetal heart's magnetic field through SQUID (Superconducting Quantum Interference Device) sensors placed on the maternal abdomen. Despite its precision, this method is costly, requires a shielded environment, and needs expert operation [4].

Fetal ECG (fECG) provides a more affordable, non-invasive alternative for continuous fetal monitoring. Nevertheless, it typically suffers from low SNR, and proper electrode placement on the maternal abdomen demands professional expertise [5].

Cardiotocography (CTG) is a widely used non-invasive standard technique employing Doppler ultrasound to monitor both FHR and uterine contractions. While it offers high accuracy and requires less technical skill, it is highly sensitive to fetal movements [7–9].

Tele-fetal monitoring (TFM) represents a promising advancement, enabling pregnant women to receive prenatal care remotely. TFM has been shown to reduce risks associated with hypertensive disorders during pregnancy [10],

provide benefits for high-risk pregnancies such as gestational diabetes, and improve access to care for women living in remote areas far from medical facilities [11].

State of the arts

Over the past decade, considerable research has focused on developing effective methods for remote fetal heart rate (fHR) extraction. One such approach is fetal heart sound (fHS) analysis, which is non-invasive, easy to apply, and cost-effective. However, fHS signals recorded from the maternal abdomen are highly susceptible to noise. Common sources of interference include fetal movements, uterine contractions, maternal digestive sounds, sensor displacement, ambient noise, maternal respiration, and maternal heart sounds [12].

The fundamental principle of fHS analysis is that the mechanical activity of the heart generates characteristic sounds associated with variations in blood flow and the opening and closing of heart valves [13]. For instance, Dia *et al*. estimated adult heart rate from phonocardiograph (PCG) signals by applying a non-negative matrix factorization (NMF) approach to the signal spectrogram and validated their results against synchronous ECG recordings [14]. Similarly, Samieinasab *et al*. [15] proposed a single-channel denoising framework for fetal PCG signals, followed by NMF decomposition in the time-frequency domain. Khandoker *et al*. developed a four-channel fPCG system and evaluated it using fECG data over a 10-minute clinical dataset, reporting significant results ($P < 0.01$ in cross-correlation analysis and <5% agreement in Bland-Altman plots) [16].

Since signal denoising remains the most challenging step in fHR extraction from fHS signals, this study presents a wavelet transformation-based denoising algorithm. The main objective is to develop an algorithm capable of accurately extracting fHR from fetal heartbeat sounds, thereby supporting tele-fetal monitoring applications.

In this study, we conducted a comprehensive investigation of 85 mother wavelets to identify the optimal approach for fHR extraction from experimental fHS signals. The wavelets included Daubechies (orders 1–45), Symlets (orders 1–20), Coiflets (orders 1–5), and Bioorthogonal wavelets (orders 1.1–6.8), tested across decomposition levels 1 to 12, resulting in a total of 1,020 configurations. The proposed methodology was implemented using a tele-monitoring ultrasound device—a pocket-sized portable Doppler system. Data were transmitted via a wired protocol and stored in a custom mobile application developed in-house, which incorporates the proposed algorithm. The long-term goal is to integrate the fHR extraction method into a mobile application for expectant mothers, as well as a cloud-based platform for gynecologists to monitor pregnancies remotely.

The remainder of this paper is organized as follows: Section 2 describes the clinical measurement procedure, data acquisition, and the applied methods for fHR extraction, including detailed explanations of pre-processing and wavelet-based filtering. Section 3 presents the analysis, validation, and discussion of the results. Finally, Sections 4 and 5 provide a discussion and conclusions, respectively.

Clinical measurement, data acquisition and methods

Clinical data were collected through simultaneous measurements using a portable (pocket-sized) ultrasound Doppler device and a standard CTG clinical system, as illustrated in **Figure 1**. The portable device employed in this study was the Baby Sound A pocket fetal Doppler from Contec Medical [17], marketed under the Baby Heart Beat brand by Sana Meditech. This device is certified with both CE and FDA medical approvals. For validation purposes, and to serve as a gold-standard reference, simultaneous measurements were performed using a clinical CTG system, specifically the Bionet FC-1400 model.

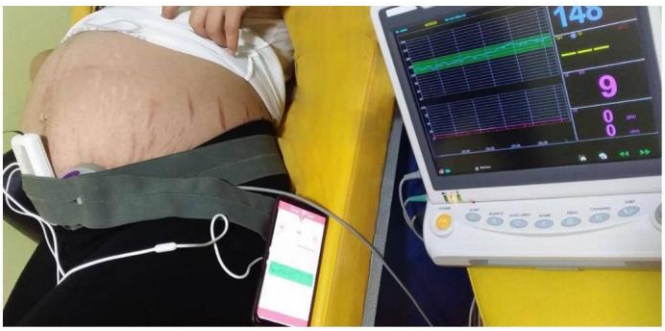

Figure 1. Clinical simultaneous measurement using the Baby Sound A pocket fetal Doppler from Contec Medical [17] and a Bionet FC-1400 CTG clinical device.

Simultaneous measurements were performed to validate the data collected by the portable Doppler device and the associated fHR processing software as an alternative to the clinical CTG system. A total of 131 samples were collected from pregnant women aged between 19 and 43 years, with a mean age of 29 years. Each sample had a duration of at least one minute and was recorded at a sampling frequency of 8 kHz.

Figure 2 provides a statistical overview of the captured clinical data. As shown in **Figure 2a**, 5% of the participants had high blood pressure, approximately 21% were diagnosed with gestational diabetes, and the remaining participants were classified as healthy. **Figure 2b** presents the pre-pregnancy Body Mass Index (BMI) distribution, ranging from a minimum of 17.44 to a maximum of 32.83, with a mean of 24.11 and a standard deviation of 4.0. The gestational age distribution is depicted in **Figure 2c**, showing that 69% of pregnancies reached full term at 40 weeks. **Figure 2d** illustrates the fetal sex distribution, with 52% male and 48% female.

For completeness, a summary of the clinical data is provided in **Table 1**, including eligibility criteria for the study population. These clinical data were recorded to enable rigorous evaluation of the proposed algorithm and to facilitate continuous improvement during its development.

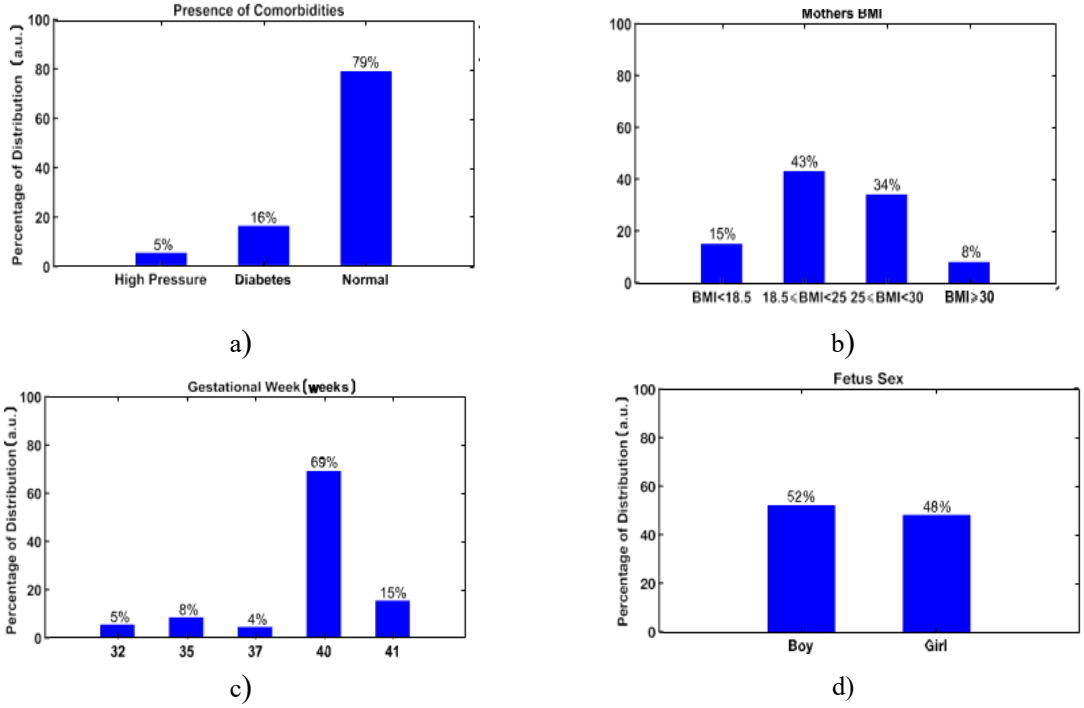

Figure 2. Statistical distribution of the clinical data for pregnant participants. Shown are (a) the proportion of normal versus high-risk pregnancies, (b) pre-pregnancy Body Mass Index (BMI) of the participants, (c) gestational age in weeks, and (d) fetal sex distribution.

Table 1. Summary of the clinical study population and eligibility criteria.

Eligible Criteria				
Age (year)	**Type of pregnancy**	**Gestation (week)**	**Body Mass Index**	**Anomaly**
from 18 to 50	singleton	greater than 32	from 15 to 45	allowed

The portable fetal monitoring device, Baby Heart Beat (Baby Sound A pocket fetal Doppler), was selected due to its superior quality, ergonomic design, and high audio fidelity compared to other similar portable devices. The device features an AUX port, enabling direct export of fetal heart sound (fHS) signals to external storage, such as a smartphone. The exported fHS signals are recorded and managed via a dedicated mobile application developed in-house by Sana Meditech.

In this study, we propose a novel method for fHR extraction from recorded fHS signals, combining adaptive band-pass filtering with wavelet transformation. The fetal heart sound signals, collected using the Doppler device from the maternal abdomen, exhibit a waveform as shown in **Figure 3**, where systolic and diastolic periods are indicated. The extraction of fHR is based on measuring the time interval between consecutive systolic peaks [18].

The overall process for algorithm development is illustrated in the flowchart of **Figure 4**, which outlines the signal processing steps for fHR extraction from fHS signals. As shown, the algorithm begins with pre-processing, followed by identification of peaks corresponding to systolic events, and concludes with fHR extraction. A final smoothing step is then applied to refine the results. The following sections provide a detailed description of each major step depicted in the flowchart.

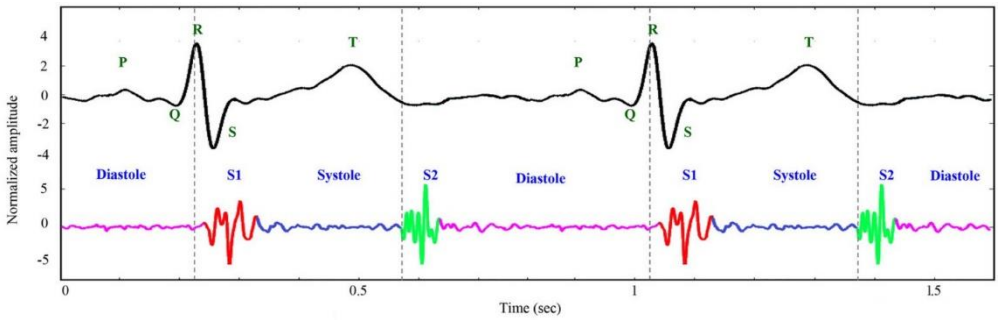

Figure 3. Illustration of a single fetal heartbeat cycle captured by an ultrasound Doppler device, highlighting the systolic and diastolic phases and their timing relative to ECG signals.

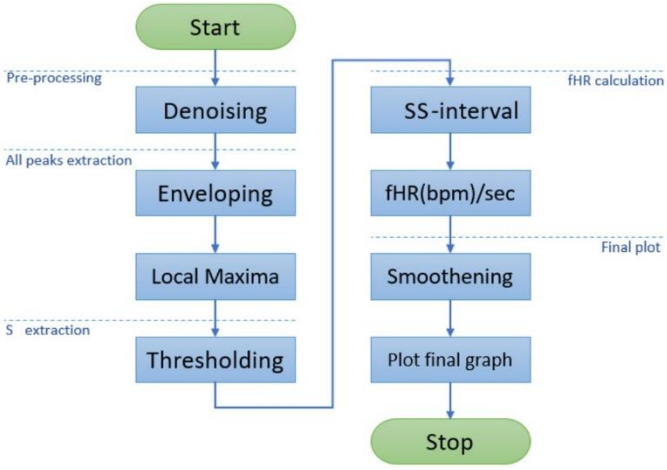

Figure 4. Flowchart illustrating the step-by-step procedure of the proposed algorithm for fetal heart rate extraction from fetal heart sound signals.

Pre-processing: pre-development algorithm with simulated data

For the development and initial testing of our algorithm, we utilized a simulated fetal heartbeat sound dataset provided by Cesarelli [19], which is publicly available on PhysioNet [20]. The dataset comprises 37 signals, each approximately 8 minutes in duration, sampled at 1 kHz. As noted by Cesarelli [19], the signals were generated with varying signal-to-noise ratios (SNRs) ranging from –26.7 dB to –4.4 dB to simulate environmental noise. Further details about this dataset are available in [20].

Fetal heart sound (fHS) signals recorded from the maternal abdomen are highly susceptible to noise, originating from fetal movements, uterine contractions, maternal abdominal sounds, sensor displacement, ambient noise, maternal respiration, and maternal heart sounds [12]. In this study, noise reduction was achieved using a wavelet transformation-based approach.

Wavelet transformation

The fundamental principle of Wavelet Transformation (WT) is to define a set of basis functions that can be stretched or compressed to capture both low- and high-frequency components of a signal. In this study, WT is employed for denoising and cleaning fetal heart sound signals. Mathematically, WT is a time-frequency analysis technique, and for an input signal x(t)x(t)x(t), it is defined as:

$$WTx(a,b)=\int_{-\infty}^{+\infty} x(t)\psi_{a,b}^{*}(t)\,dt, a\neq 0 \quad WT_{x}(a,b) = \int_{-\infty}^{+\infty} x(t) \psi_{a,b}^{*}(t) \, dt, \quad a \neq 0 \quad (1)$$

where the basic wavelet function $\psi_{a,b}(t)$ is characterized by scale (a) and time-shift (b) parameters:

$$\psi_{a,b}(t)=\frac{1}{\sqrt{a}}\psi\left(\frac{t-b}{a}\right) \quad \psi_{a,b}(t) = \frac{1}{\sqrt{a}} \psi\left(\frac{t-b}{a}\right) \quad (2)$$

This function $\psi_{a,b}(t)$ is also used for signal decomposition. A key challenge in applying WT for denoising lies in selecting the optimal mother wavelet for the specific application. To systematically determine the most suitable mother wavelet, several properties are considered, including vanishing moments, support size, regularity, orthogonality, biorthogonality, energy distribution, symmetry, and suitability for discrete signal implementation [21, 22].

Table 2 provides a summary of the 14 different families of mother wavelets investigated in this study. The following section details the procedure for selecting the optimal mother wavelet for fetal heart sound signal denoising.

Table 2. A Summary of Different Mother Wavelets' Properties.

Mother Wavelet	Compact Support	Vanishing Moment	Regularity	Orthogonal	Bio Orthogonal	Symmetric	Energy	Discrete Wavelet	Continues Wavelet	References
HAAR	✓	1	×	✓	✓	✓	✓	✓	✓	[23]
Daubechies	✓	N	0.2N	✓	✓	×	✓	✓	✓	[23]
Symlets	✓	N	-	✓	✓	near	✓	✓	✓	[23]
Coiflets	✓	2N	-	✓	✓	near	✓	✓	✓	[23]
Biorthogonal	✓	Nr	Nr-1	×	✓	✓	✓	✓	✓	[23]
Fejer-Korovkin	✓	N	-	✓	×	×	✓	✓	✓	[24, 25]
Meyers	×	N	inf	✓	✓	✓	✓	*	✓	[23]
Gaussian	×	-	-	×	×	**	×	×	✓	[26]
Mexican hat	×	2	-	×	×	✓	×	×	✓	[23, 27]
Morlet	×	-	-	×	×	✓	×	×	✓	[23]
Complex Gaussian	×	-	-	×	×	**	×	×	✓	[26]
Shannon	×	N	-	×	×	✓	×	×	✓	[28]
Freq. B-Spline	×	-	-	×	×	✓	×	×	✓	[28]
Complex Morlet	×	-	-	×	×	✓	×	×	✓	[28]

* Fast wavelet transform implementation is possible, but not available for this case.

** These wavelets exhibit symmetry when their order is an even number.

Mother wavelet selection

The procedure for selecting the most suitable mother wavelet is based on evaluating each wavelet's properties **(Table 2).** Initially, wavelets that are not suitable for fetal heart sound (fHS) denoising are excluded. For example, wavelets that do not preserve signal energy, such as non-orthogonal types—including Gaussian, Mexican Hat, Morlet, Complex Gaussian, Shannon, Frequency B-Spline, and Complex Morlet—are discarded. Additionally, wavelets must support discrete wavelet transform; thus, the Meyer family, which cannot perform fast WT for discrete signals, is also excluded.

Wavelets with moderate complexity and a minimum number of vanishing moments are preferred, as these can represent complex functions with fewer coefficients [29]. Based on these criteria, Daubechies, Symlets, Coiflets, and Biorthogonal wavelets were selected for investigation. Specifically, the study considered 85 wavelets: db1–db45, sym1–sym20, coif1–coif5, and bior1.1–bior6.8.

To identify the optimal wavelet, two key metrics were used: energy and entropy. Energy measures the similarity between the signal and the wavelet. The energy of detail coefficients at level jjj is defined as:

$$Ej=\sum k|Cj(k)|2E_j = \sum_{k} |C_j(k)|^2Ej=k\sum|Cj(k)|2 \quad (3)$$

where Cj(k)C_j(k)Cj(k) represents the wavelet coefficients at level jjj. The total energy is then given by:

$$Etot=\sum jEjE_\text{tot} = \sum_j E_jEtot=j\sum Ej \quad (4)$$

The relative wavelet energy, which assesses similarity between different signal segments, is defined as:

$$pj=EjEtotp_j = \frac{E_j}{E_\text{tot}}pj=EtotEj \quad (5)$$

Entropy quantifies the accuracy of signal reconstruction and the information lost due to the chosen wavelet:
0

$$H(j)=-\sum jpj2log⁡(pj2)H(j) = - \sum_j p_j^2 \log(p_j^2)H(j)=−j\sum pj2log(pj2) \quad (6)$$

The ratio of relative wavelet energy to entropy (RWEER) provides a measure of how closely a wavelet resembles the original signal:

$$RWEER(j)=E(j)H(j)\text{RWEER}(j) = \frac{E(j)}{H(j)}RWEER(j)=H(j)E(j) \quad (7)$$

In this study, RWEER was computed up to level j=12j = 12j=12 using 215 abdominal fHS segments for all 85 mother wavelets. The first row of **Figure 5** shows that the highest RWEER occurs at level 4; hence, this decomposition level was chosen. RWEER was then calculated at level 4 to determine the optimal mother wavelet. The bottom of **Figure 5** presents a boxplot of the RWEER distribution across all 215 segments for each wavelet. The red dashed line indicates execution time, while the black dashed line represents the ratio of mean to standard deviation of RWEER. Wavelet numbers on the x-axis correspond to Daubechies (1–45), Symlets (46–65), Coiflets (66–70), and Biorthogonal (71–85).
Based on this analysis, Biorthogonal 2.2 (bior2.2, wavelet number 74) was selected for fHS denoising, as it exhibited the highest mean-to-standard deviation ratio, consistent repeatability across segments, and low computational time.

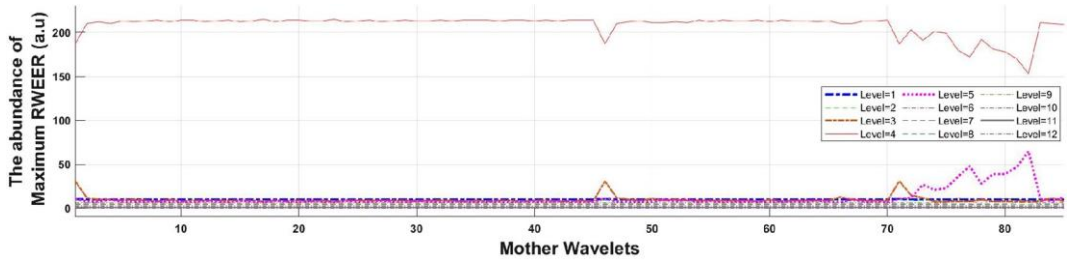

a)

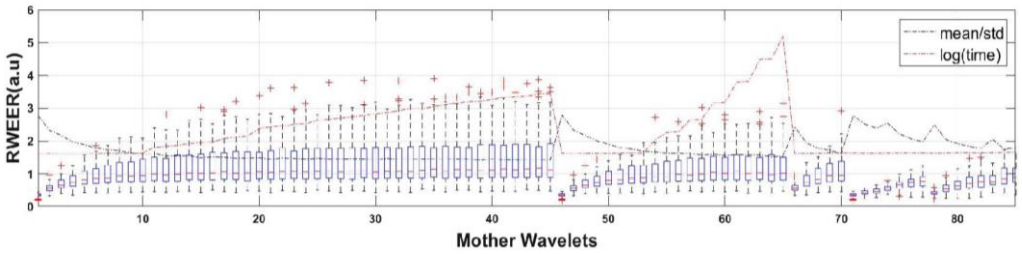

b)

Figure 5. Distribution of RWEER for 85 mother wavelets, including Daubechies (db1–db45), Symlets (sym1–sym20), Coiflets (coif1–coif5), and Biorthogonal (bior1.1–bior6.8). a)Top row**:** Effect of wavelet decomposition levels on the maximum RWEER, indicating that level j=4j = 4j=4 yields the highest values. b)Bottom row**:** RWEER for 215 fHS sections at level j=4j = 4j=4 across different mother wavelets. The red

dash-dot line represents the algorithm's execution time for each wavelet, while the black dash-dot line shows the mean-to-standard deviation ratio of RWEER for all sections. Outliers are marked with red plus symbols.

Based on this analysis, all fHS signal decomposition, denoising, and reconstruction in this study were performed using Biorthogonal 2.2 (bior2.2) with 4 levels of decomposition. An example comparing a noisy fHS signal to its denoised version is shown in **Figure 6**. **Figure 6a** displays a 1-second segment of the original fHS signal, **Figure 6b** shows the denoised signal obtained using the proposed method, and **Figure 6c** illustrates the extracted systolic (S) peaks.

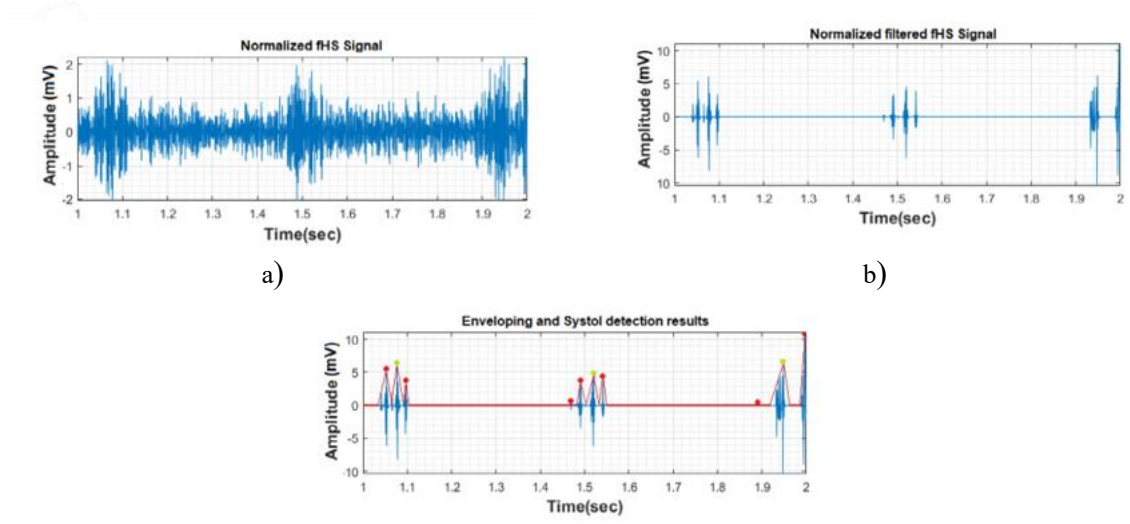

Figure 6. Example of an fHS signal before and after denoising. (a) One-second segment of the original fHS signal, (b) the denoised signal obtained using the proposed wavelet-based filtering method, and (c) the extracted S-peaks. In (c), the red curve represents the computed envelope, red markers indicate all detected local maxima, and green markers highlight the selected S-peaks.

Systole extraction

The identification of systolic peaks is a key step in estimating the fetal heart rate (fHR), as illustrated in **Figure 3**. In fetal heart sound (fHS) recordings, the temporal gap between systole (S) and diastole (D) is significantly shorter than in adult cardiac cycles. Given that diastole typically lasts longer than systole, a diastolic peak generally appears at least 100 ms after the preceding S and no more than 200 ms before the next S [30]. Based on this physiological constraint, the extraction strategy involves two stages: first detecting all potential peaks (both S and D), and then isolating the true systolic peaks.

To identify every candidate peak, the signal is processed by computing its envelope followed by detection of local maxima. As illustrated in **Figure 6**, these maxima represent possible S–D events. The subsequent selection of true S-peaks relies on expected fetal cardiac cycle durations: a normal cycle is approximately 430 ms, with a typical range of 375–545 ms [31]. Accordingly, a threshold-based decision rule is applied to determine which of the detected candidates correspond to systole. These selected systolic peaks are then used for fHR computation. An example outcome is shown in **Figure 6c**, where the envelope is plotted in red, all detected candidates appear as red markers, and the final chosen S-peaks are highlighted in green.

fHR cardiograph visualization

Since the interval between two consecutive systolic peaks (S–S interval) in an fHS signal reflects the combined duration of systole and diastole [32], the fetal heart rate can be derived using Eq. (8):

fHR (bpm)=60Tss (sec)(8)\text{fHR (bpm)} = \frac{60}{T_{ss} \, (\text{sec})} \tag{8}fHR (bpm)=Tss (sec)60((8)

where TssT_{ss}Tss denotes the time difference between successive systolic peaks, and the resulting fHR is expressed in beats per minute (bpm).

To generate a clinically meaningful and easy-to-read fHR trace, additional smoothing procedures are applied. Beat-to-beat fHR estimates may occasionally exhibit abrupt fluctuations due to noise, motion artifacts, or transient signal loss. To mitigate these effects, we reduce high- and low-frequency noise components and correct outliers using a dedicated correction algorithm. These refinements are intended solely for visualization in the cardiograph to avoid presenting unnecessarily erratic trends that may cause concern for end users.

In constructing the cardiograph, we also preserve continuity of the displayed fHR values. When brief signal dropouts occur, the nearest valid fHR measurement obtained from the clinical reference device is retained to avoid artificial gaps in the display.

To further stabilize the plotted fHR curve, smoothing methods such as moving median and moving average filters are employed. These approaches help reduce variability arising from spontaneous fetal movements or residual artifacts, resulting in a more coherent and interpretable cardiograph signal.

Analysis and validation of results

The analysis and validation procedures in this work were conducted on a personal computer using MATLAB R2020a, and consisted of two primary experimental stages. In the first stage, we employed a publicly available simulated fetal heart sound (fHS) dataset [19] to develop and test the algorithm. This dataset includes 37 synthetic fetal phonocardiogram (fPCG) recordings, each lasting at least eight minutes and sampled at 1 kHz.

To assess the accuracy of the proposed method, we compared the algorithm-derived beat-to-beat fHR values with the reference (baseline) heart rates provided in the dataset. Performance evaluation was carried out using beat-to-beat correlation analysis and Bland–Altman assessment [33], enabling a quantitative comparison of agreement between the estimated and reference fHR values.

Analysis over simulated data

To begin, we evaluated the performance and accuracy of the algorithm using a single fHS recording approximately eight minutes in duration. **Figure 7** presents the resulting cross-correlation analysis along with the Bland–Altman assessment, a standard statistical method for examining agreement between two paired measurements on the same scale. As shown, the computed p-value is <0.0001, indicating strong statistical significance since it is well below the conventional 0.05 threshold. A 95% confidence interval was applied in this analysis, and the signal-to-noise ratio (SNR) for the examined recording is noted in the figure caption.

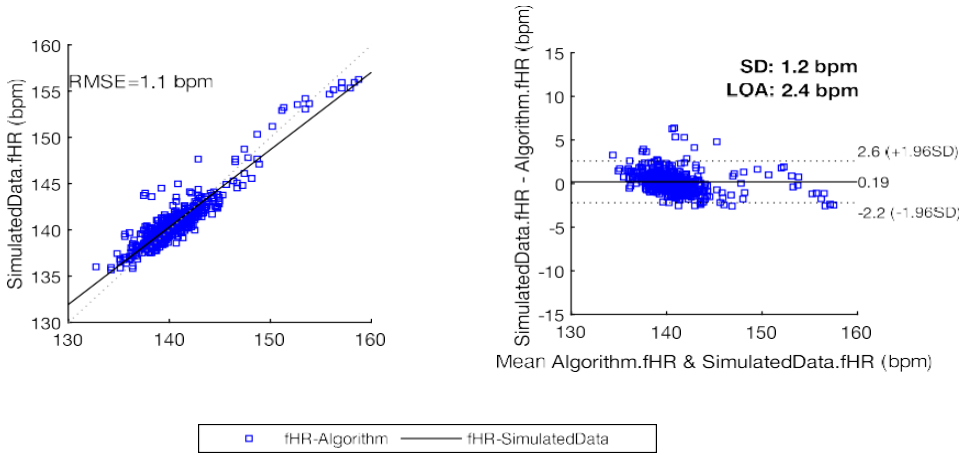

Figure 7. shows the results for a single simulated recording of approximately eight minutes. The left panel illustrates the beat-to-beat cross-correlation between the algorithm-derived fHR and the reference signal, while the right panel presents the corresponding Bland–Altman analysis. For this example, the SNR is −26.7 dB, and the p-value is <0.0001, confirming strong statistical significance in the agreement between the two measurements.

In the second stage of evaluation, we assessed the algorithm's performance across all 37 simulated signals to determine overall accuracy and robustness. Using a 95% confidence interval, the average p-value across the

dataset was <0.0008, indicating consistently significant agreement with the reference values **(Figure 8)**. Additionally, the mean root-mean-square error (RMSE) across all signals was 2.74 bpm. **Figure 8** summarizes these results, displaying a detailed performance breakdown for each individual simulated recording.

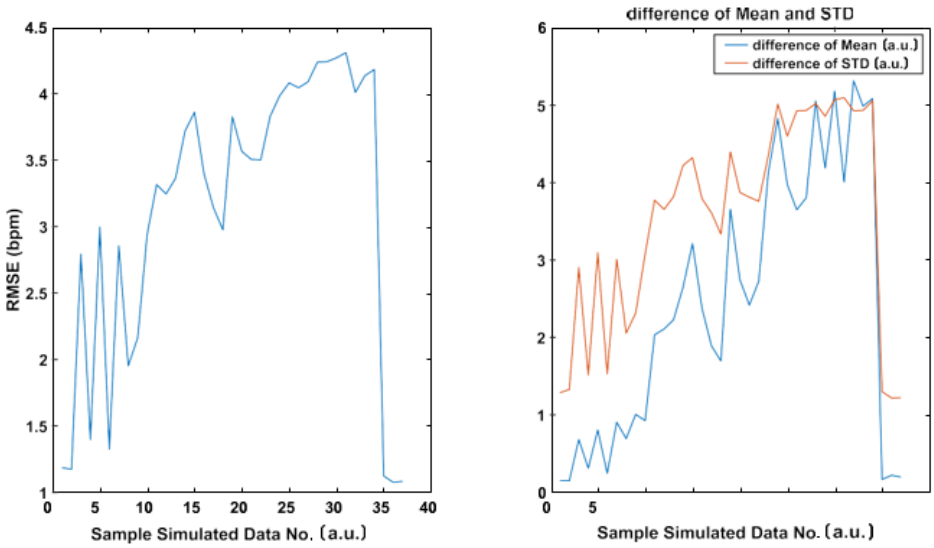

Figure 8. presents the statistical evaluation of the algorithm across the full set of simulated recordings. The overall performance is highly consistent, with an average p-value of <0.0008. The left panel displays the root mean square error (RMSE) for each signal, while the right panel illustrates the mean difference and standard deviation between the algorithm-estimated fHR and the baseline reference values.

The average accuracy of the algorithm is computed according to:

$$\text{Average Accuracy} = \frac{1}{N_T} \sum_{i=1}^{K} \left(\frac{NE_i}{60} \right) \quad (9)$$

where NTN_TNT denotes the total number of samples and NEiNE_iNEi represents the number of correctly estimated beats for the iii-th recording.

Analysis over clinical data

The proposed algorithm is subsequently evaluated and fine-tuned using the clinical dataset collected through simultaneous measurements from the portable fetal Doppler and a clinical-grade CTG device. For this validation, the Baby Heart Beat (Baby Sound A) portable Doppler is used to acquire fHS signals, which are recorded through the accompanying mobile application. In parallel, a Bionet FC-1400 clinical monitor records the reference fetal heart rate. The clinical device exports the fHR trace as an image **(Figure 9a)**, in which the y-axis represents heart rate in beats per minute (bpm) and the x-axis indicates time in seconds. Each grid cell corresponds to 10 bpm vertically and 10 seconds horizontally.

To obtain the reference fHR numerically, image-processing routines implemented in MATLAB are applied to extract the clinical fHR curve from the exported image **(Figure 9b and 9c)**. According to clinical standards [34], an algorithm-derived fHR value is considered acceptable if it lies within ±7 bpm of the value reported by the validated clinical device. This acceptance band is highlighted in **Figure 9d** (green region). After defining this confidence interval for the baseline measurement, the fHR estimated by our algorithm is superimposed onto the clinical signal **(Figure 9e)** to assess agreement and quantify the error rate.

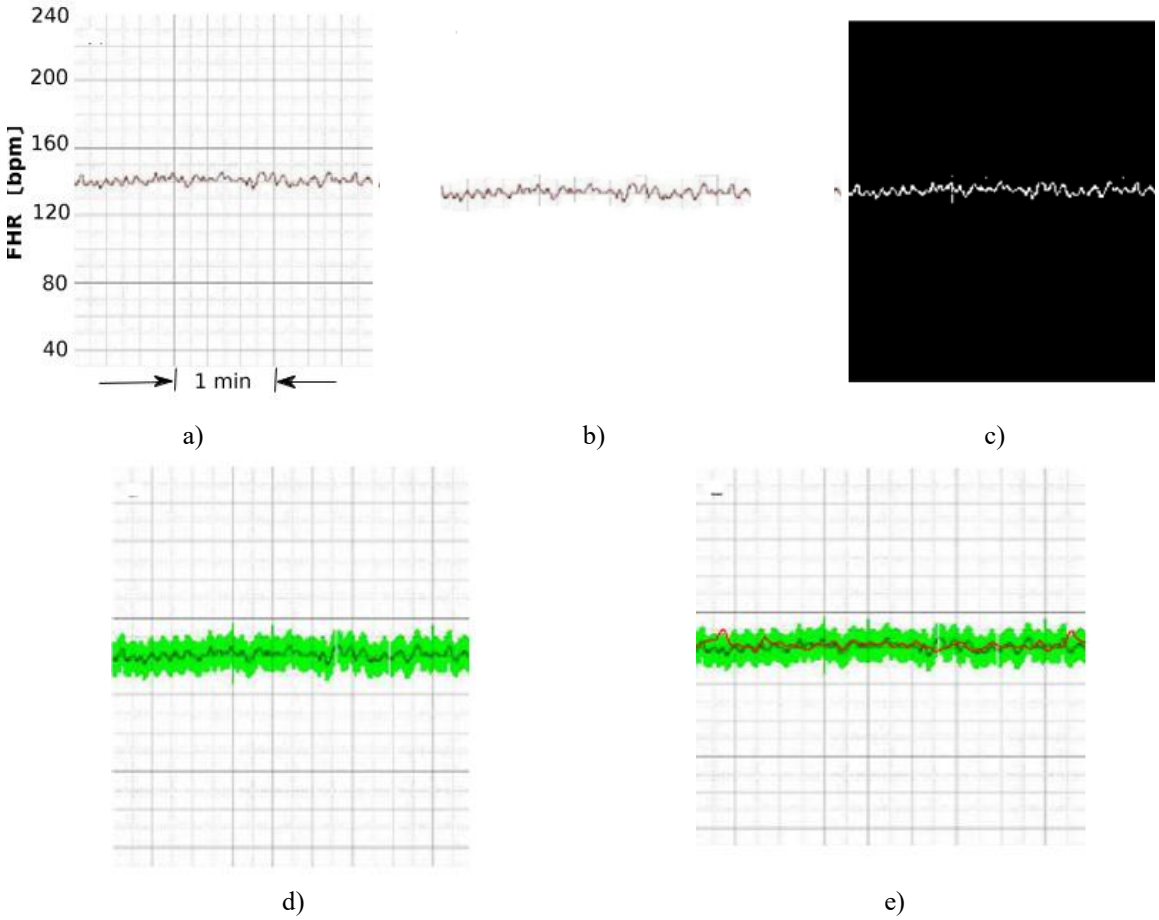

Figure 9. illustrates how image-processing techniques are employed to validate the proposed algorithm. (a) The original fHR trace exported from the clinical device. (b, c) Extraction of the clinical fHR curve using MATLAB-based processing. (d) Definition of the medical acceptance interval (±7 bpm). (e) Superimposition of the algorithm-generated fHR (shown in red) for comparison.

Figure 10 presents an additional example in which discrepancies between the algorithm output and the clinical reference are highlighted with red arrows, demonstrating how these detected errors guide further refinement and optimization of the algorithm's performance.

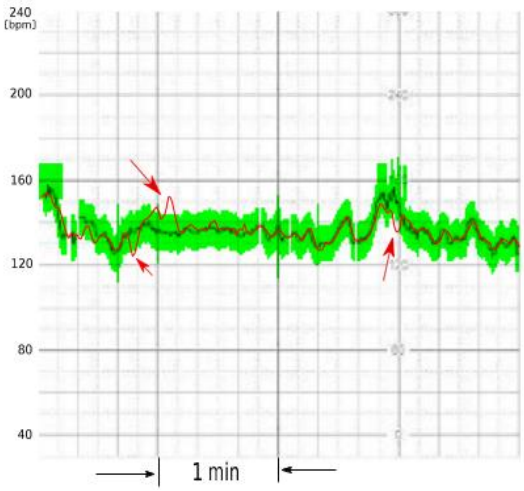

Figure 10. presents an example comparing the algorithm-generated fHR trace (red) with the clinical reference signal (black). The green band indicates the accepted confidence interval (±7 bpm), and the detected outliers are marked with red arrows.

In this study, each clinical recording used for validation has a duration of at least one minute. To assess the performance of the proposed algorithm, the average accuracy is computed using Eq. (9). Let NEiNE_iNEi denote the number of errors in the *i*-th signal, with each signal spanning 60 seconds, and let NTN_TNT be the total dataset duration. With 131 clinical samples, NT=7860N_T = 7860NT=7860 seconds (131 × 60). Across all measurements, only 390 errors were detected, corresponding to an overall accuracy of **95.03%** and an error rate of 4.96%.

Figure 11a illustrates the distribution of median fHR values alongside the associated error rates. To further characterize variability within each measurement, **Figure 11b** provides the quantile distribution of fHR values using a boxplot, which visualizes beat-to-beat fluctuations and the statistical characteristics of each clinical sample.

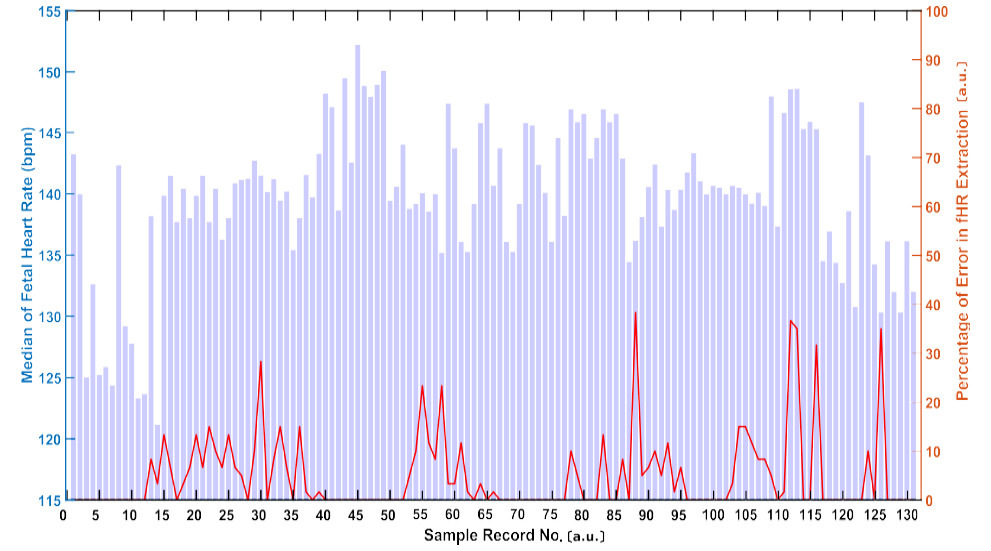

a)

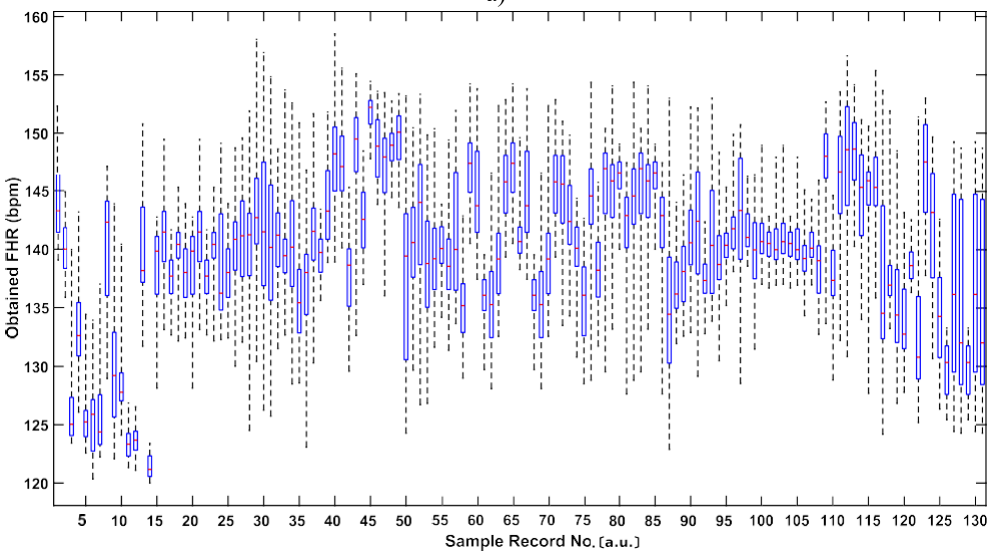

b)

Figure 11 presents the error analysis for each clinical sample. (a) The orange line indicates the percentage of errors per sample, while the purple bars show the distribution of median fHR values in bpm. (b) The boxplot illustrates the quantile distribution of fHR measurements, highlighting variability within each recording.

It should be noted that elevated error rates in certain samples are primarily due to missing data points from the clinical device, which is a common limitation. In these cases, our algorithm often outperforms the standard clinical system. With further refinement and the incorporation of additional clinical datasets, we anticipate that this algorithm could form the basis of a highly advanced fetal monitoring solution.

Results and Discussion

To evaluate the performance of the proposed algorithm relative to existing approaches, several commonly used wavelet families—including db1, db5, db6, sym1, sym7, coif2, and coif4—were selected for comparison. The analysis was conducted using all 37 signals from the simulated dataset. fHR extraction accuracy was computed following denoising with each wavelet, and the results are summarized in **Figure 12**. The figure demonstrates that the proposed method achieves superior performance in the majority of cases compared to the alternative wavelet-based approaches.

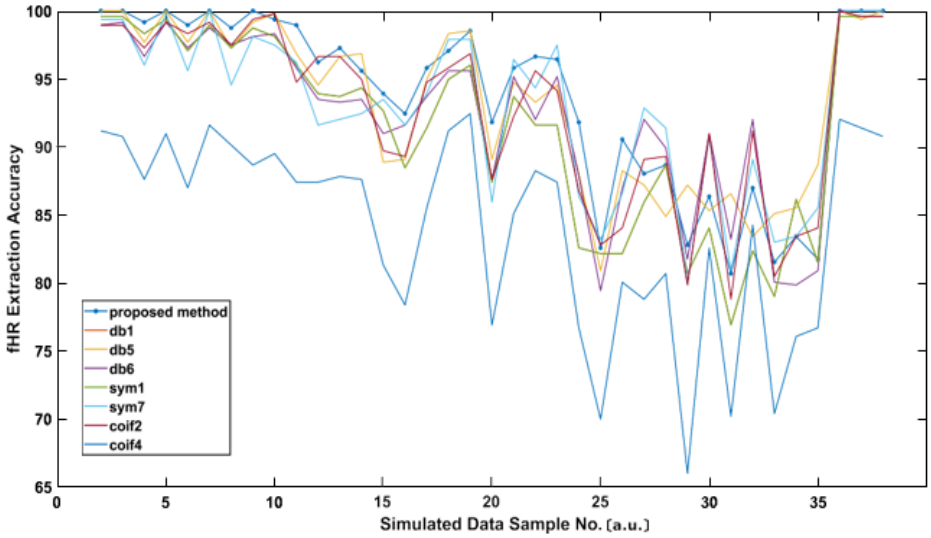

Figure 12. presents a comparison of the proposed algorithm with previously reported methods [35, 36].

Fetal heart sound (fHS) signals are often highly noisy due to multiple sources, including maternal and fetal activity as well as environmental factors. Effective denoising is therefore critical for accurate fetal heart rate (fHR) extraction. In this study, we conducted a comprehensive investigation of fHS denoising using wavelet transformation techniques. We evaluated 1020 configurations covering four mother wavelet families: Daubechies (orders 1–45), Coiflets (orders 1–5), Symlets (orders 1–20), and Biorthogonal (orders 1.1–6.8), across decomposition levels 2–12.

Additionally, over 131 minutes of clinical data were collected from 131 pregnant women, encompassing a wide range of BMIs, gestational weeks, and risk factors such as diabetes and hypertension. The results demonstrate that the proposed algorithm performs robustly in real-world clinical settings. Furthermore, the algorithm is embedded in software connected to a pocket-size Doppler device, enabling remote monitoring of high-risk pregnancies and potentially reducing the clinical workload for healthcare providers.

Conclusion

Fetal heart sound (fHS) signals are typically low in amplitude and often obscured by high-amplitude noise originating from maternal respiration, fetal movements, and other environmental sources. In this study, we developed an algorithm to estimate fetal heart rate (fHR) from fHS recordings. The process begins with wavelet-based denoising during the pre-processing stage, followed by the extraction of systolic and diastolic peaks using a combination of signal enveloping and local maxima detection. True systolic peaks are then selected based on the temporal relationship between systolic and diastolic events, and fHR is computed from the intervals between consecutive systolic peaks.

Evaluation against both simulated and clinical datasets demonstrates that the proposed method provides accurate and reliable fHR estimation. Looking forward, by acquiring more extensive annotated datasets, including recordings with abnormal cardiac patterns, this framework could be extended to support fetal anomaly detection using advanced machine learning techniques.

Acknowledgments: The project is supported by the Spanish government R&D project CDTI Neotec No. SNEO-20201283, and Universitat Politècnica de Catalunya. The authors are also grateful to the team of Mehr-e-Madar hospital and the dedicated gynecology clinic, for the clinical data acquisition.

Conflict of Interest: None

Financial Support: None

Ethics Statement: None

References

1. S.M. Abman, Fetal and Neonatal Physiology, Elsevier Publisher, 2011.
2. N.E. Reichman, H. Corman, K. Noonan, O. Schwartz-Soicher, Parity and pregnancy outcomes, Rev. Econ. Househ. 8 (2) (2010) 171–297.
3. R.M. Grivell, Z. Alfirevic, G.M. Gyte, D. Devane, Antenatal cardiotocography for fetal assessment, Cochrane Database of Systematic Reviews 9.
4. M. Peters, J. Crowe, J.-F. Piéri, H. Quartero, B. Hayes-Gill, D. James, J. Stinstra, S. Shakespeare, Monitoring the fetal heart non-invasively: a review of methods.
5. M. Nassit, H. Berbia, Non-invasive technologies of fetal heart rate diagnosis, in: 2015 Third World Conference on Complex Systems (WCCS), IEEE, 2015, pp. 1–5.
6. L.W. Organ, Scalp lead fetal electrocardiography, Canadian Medical Association Journal 98 (4) (1968) 199.
7. M.P. Nageotte, Fetal heart rate monitoring, in: Seminars in Fetal and Neonatal Medicine, vol. 20, Elsevier, 2015, pp. 144–148.
8. T.Y. Euliano, M.T. Nguyen, S. Darmanjian, S.P. McGorray, N. Euliano, A. Onkala, A.R. Gregg, Monitoring uterine activity during labor: a comparison of 3 methods, American journal of obstetrics and gynecology 208 (1) (2013) 66–e1.
9. S. Alnuaimi, S. Jimaa, Y. Kimura, L.J. Hadjileontiadis, A.H. Khandoker, Fetal car- diac timing events estimation from Doppler ultrasound signal cepstrum analysis, in: 2019 41st Annual International Conference of the IEEE Engineering in Medicine and Biology Society (EMBC), IEEE, 2019, pp. 4677–4681.
10. D. Lanssens, S. Vonck, V. Storms, I.M. Thijs, L. Grieten, W. Gyselaers, The impact of a remote monitoring program on the prenatal follow-up of women with gestational hypertensive disorders, European Journal of Obstetrics & Gynecology and Repro- ductive Biology 223 (2018) 72–78.
11. J.F. Van Den Heuvel, T.K. Groenhof, J.H. Veerbeek, W.W. Van Solinge, A.T. Lely, A. Franx, M.N. Bekker, eHealth as the next-generation perinatal care: an overview of the literature, Journal of medical Internet research 20 (6) (2018) e9262.
12. Strazza, A. Sbrollini, V. Di Battista, R. Ricci, L. Trillini, I. Marcantoni, M. Moret- tini, S. Fioretti, L. Burattini, PCG-delineator: an efficient algorithm for automatic heart sounds detection in fetal phonocardiography, in: 2018 Computing in Cardiol- ogy Conference (CinC), vol. 45, IEEE, 2018, pp. 1–4.
13. H. Tang, J. Zhang, J. Sun, T. Qiu, Y. Park, Phonocardiogram signal compression using sound repetition and vector quantization, Computers in biology and medicine 71 (2016) 24–34.
14. N. Dia, J. Fontecave-Jallon, P.-Y. Guméry, B. Rivet, Heart rate estimation from phonocardiogram signals using non-negative matrix factorization, in: ICASSP 2019- 2019 IEEE International Conference on Acoustics, Speech and Signal Processing (ICASSP), IEEE, 2019, pp. 1293–1297.
15. M. Samieinasab, R. Sameni, Fetal phonocardiogram extraction using single channel blind source separation, in: 2015 23rd Iranian Conference on Electrical Engineering, IEEE, 2015, pp. 78–83.
16. Khandoker, E. Ibrahim, S. Oshio, Y. Kimura, Validation of beat by beat fetal heart signals acquired from four-channel fetal phonocardiogram with fetal electrocardio- gram in healthy late pregnancy, Scientific reports 8 (1) (2018) 1–11.
17. C.M. Company, Baby sound a pocket fetal Doppler device, URL, https:// www.contecmed.com/index.php?page=shop.product_details&flypage=flypage. tpl&product_id=66&category_id=14&option=com_virtuemart&Itemid=606.
18. S. Schmidt, C. Holst-Hansen, C. Graff, E. Toft, J. Struijk, Detection of coronary artery disease with an

electronic stethoscope, in: 2007 Computers in Cardiology, IEEE, 2007, pp. 757–760.
19. M. Cesarelli, M. Ruffo, M. Romano, P. Bifulco, Simulation of foetal phonocardio- graphic recordings for testing of FHR extraction algorithms, Computer methods and programs in biomedicine 107 (3) (2012) 513–523.
20. Simulated fetal phonocardiograms data set, URL, https://physionet.org/content/ simfpcgdb/1.0.0/.
21. Y. Yang, Z. Peng, W. Zhang, G. Meng, Parameterised time-frequency analysis meth- ods and their engineering applications: a review of recent advances, Mechanical Systems and Signal Processing 119 (2019) 182–221.
22. M. Rhif, A. Ben Abbes, I.R. Farah, B. Martínez, Y. Sang, Wavelet transform appli- cation for/in non-stationary time-series analysis: a review, Applied Sciences 9 (7) (2019) 1345.
23. Daubechies, Ten Lectures on Wavelets, Society for Industrial and Applied Mathe- matics, 1992.
24. M. Nielsen, On the construction and frequency localization of finite orthogonal quadrature filters, Journal of Approximation Theory 108 (1) (2001) 36–52.
25. C.-C. Chen, F.R. Tsui, Comparing different wavelet transforms on removing elec- trocardiogram baseline wanders and special trends, BMC medical informatics and decision making 20 (11) (2020) 1–10.
26. S. Mallat, A Wavelet Tour of Signal Processing, Elsevier, 1999.
27. G. Leigh, Fast FIR algorithms for the continuous wavelet transform from constrained least squares, IEEE Transactions on Signal Processing 61 (2013) 28–37.
28. Teolis, J.J. Benedetto, Computational Signal Processing with Wavelets, vol. 182, Springer, 1998.
29. T. Omari, F. Bereksi-Reguig, An automatic wavelet selection scheme for heart sounds denoising, in: 2014 International Work-Conference on Bioinformatics and Biomedi- cal Engineering, 2014, pp. 1450–1462.
30. M. Salwani, Y. Jasmy, Relative wavelet energy as a tool to select suitable wavelet for artifact removal in EEG, in: 2005 1st International Conference on Computers, Com- munications, & Signal Processing with Special Track on Biomedical Engineering, IEEE, 2005, pp. 282–287.
31. E. Koutsiana, L. Hadjileontiadis, I. Chouvarda, A. Khandoker, Fetal heart sounds detection using wavelet transform and fractal dimension, Frontiers Bioengineering and Biotechnology 5 (2017) 1–8.
32. F. Kovács, C. Horváth, Á.T. Balogh, G. Hosszú, Fetal phonocardiography—past and future possibilities, Computer methods and programs in biomedicine 104 (1) (2011) 19–25.
33. D. Giavarina, Understanding bland Altman analysis, Biochemia medica 25 (2) (2015) 141–151.
34. B. Hayes-Gill, S. Hassan, F.G. Mirza, S. Ommani, J. Himsworth, M. Solomon, R. Brown, B.S. Schifrin, W.R. Cohen, Accuracy and reliability of uterine contraction identification using abdominal surface electrodes, Clinical Medicine Insights: Wom- en's Health 5 (2012), CMWH–S10444.
35. S. Tomassini, A. Strazza, A. Sbrollini, I. Marcantoni, M. Morettini, S. Fioretti, L. Burattini, Wavelet filtering of fetal phonocardiography: a comparative analysis, Mathematical Biosciences and Engineering 16 (5) (2019) 6034–6046.
36. P.C. Adithya, R. Sankar, W.A. Moreno, S. Hart, Trends in fetal monitoring through phonocardiography: challenges and future directions, Biomedical Signal Processing and Control 33 (2017) 289–305.